iMSC exosome delivers hsa-mir-125b-5p and strengthens acidosis resilience through suppression of ASIC1 protein in cerebral ischemia-reperfusion

Kai Dong[1], **Fangyan Chen**[2], **Liang Wang**[3], **Chengyu Lin**[3], **Mingyao Ying**[4], **Bingnan Li**[5,6,7,*], **Tao Huang**[5,*], and **Shuyan Wang**[8,*]

From the [1]Department of Neurology, Beijing Anding Hospital, Capital Medical University, Beijing, China; [2]Beijing Hospital, National Center of Gerontology, Beijing, China; [3]Department of Quality Control, Guidon Pharmaceutics, Beijing, China; [4]Department of Neurology, Johns Hopkins University School of Medicine, Baltimore, Maryland, USA; [5]Medical Integration and Practice Center, Cheeloo College of Medicine, Shandong University, Jinan, Shandong, China; [6]State Key Laboratory of Medical Molecular Biology, Institute of Basic Medical Sciences, Chinese Academy of Medical Sciences, School of Basic Medicine, Peking Union Medical College, Beijing, China; [7]Neuroscience Center, Chinese Academy of Medical Sciences, Beijing, China; [8]Department of Neurology, Xuanwu Hospital, Capital Medical University, Beijing, China

Reviewed by members of the JBC Editorial Board. Edited by Kirill Martemyanov

Acid-sensing ion channel 1 (ASIC1) is critical in acidotoxicity and significantly contributes to neuronal death in cerebral stroke. Pharmacological inhibition of ASIC1 has been shown to reduce neuronal death. However, the potential of utilizing exosomes derived from pluripotent stem cells to achieve inhibition of *Asic1* remains to be explored. Developing qualified exosome products with precise and potent active ingredients suitable for clinical application is also ongoing. Here, we adopt small RNA-seq to interrogate the miRNA contents in exosomes of pluripotent stem cell induced mesenchymal stem cell (iMSC). RNA-seq was used to compare the oxygen-glucose deprivation–damaged neurons before and after the delivery of exosomes. We used Western blot to quantify the Asic1 protein abundance in neurons before and after exosome treatment. An *in vivo* test on rats validated the neuroprotective effect of iMSC-derived exosome and its active potent miRNA hsa-mir-125b-5p. We demonstrate that pluripotent stem cell–derived iMSCs produce exosomes with consistent miRNA contents and sustained expression. These exosomes efficiently rescue injured neurons, alleviate the pathological burden, and restore neuron function in rats under oxygen-glucose deprivation stress. Furthermore, we identify hsa-mir-125b-5p as the active component responsible for inhibiting the Asic1a protein and protecting neurons. We validated a novel therapeutic strategy to enhance acidosis resilience in cerebral stroke by utilizing exosomes derived from pluripotent stem cells with specific miRNA content. This holds promise for cerebral stroke treatment with the potential to reduce neuronal damage and improve clinical patient outcomes.

Ischemic stroke is one of the leading causes of death and high disability worldwide. Clinical outcomes of out-of-hospital brain stroke patients remain disappointingly poor, with limited treatment options. Ischemia and reperfusion lead to the activation of multiple cell death programs, including apoptosis, necrosis, autophagy, pyroptosis, and necroptosis. Ischemic stroke is a primary global health concern, being one of the leading causes of death and disability. Despite extensive efforts, the clinical outcomes for out-of-hospital brain stroke patients remain unsatisfactory, with limited treatment options available. The pathophysiology of ischemic stroke involves complex cellular processes triggered by ischemia and subsequent reperfusion, leading to the activation of multiple cell death pathways, such as apoptosis, necrosis, autophagy, pyroptosis, and necroptosis. Understanding and effectively targeting these cell death programs present critical challenges in improving stroke treatments. Meanwhile, one major challenge in treating ischemic stroke is achieving safe and effective drug delivery. Mesenchymal stem cell (MSC)-derived exosomes have emerged as a promising therapeutic approach due to their low immunogenicity and potential benefits in ischemia-reperfusion syndrome. Exosomes, a subgroup of extracellular vesicles (MVs) with diameters ranging from 30 to 150 nm, can be internalized by neighbouring or distant cells, subsequently influencing recipient cells. The transfer of miRNA cargo between cells is considered a plausible mechanism underlying the therapeutic effects of exosomes. Numerous miRNAs, prominently enriched in MSC-derived exosomes, have been reported to attenuate ischemia-reperfusion injury in the kidney, myocardial infarction, and ischemic stroke (1–3).

miRNAs are single-stranded molecules consisting of 20 to 25 nt and can target multiple genes through binding to the 3'-UTR. miRNAs delivered by exosomes play a role in repressing functional gene transcripts related to apoptosis, survival, and differentiation. Prior research has demonstrated that MSC-exosomes deliver miRNAs, leading to improvements in cellular repair, neurite branching and outgrowth, angiogenesis, and suppression of neuroinflammation (4–7). However, the

exact underlying mechanism remains elusive. Therefore, there is an urgent need to identify the active components of exosomes and assess their therapeutic effects on ischemia-reperfusion injury. Potent miRNA species or families must be systematically screened, identified, and validated in this context. Moreover, defining and quantifying features that characterize exosome identity, purity, sterility, potency, and stability are crucial to ensuring batch-to-batch reproducibility of therapeutic efficacy. Addressing these questions will pave the way for further clinical trials, bringing us closer to a more comprehensive understanding of MSC-derived exosomes' therapeutic potential in ischemic stroke management.

Within seconds of circulatory arrest, brain function ceases, indicating the extremely short temporal tolerance of the human brain to ischemia. The primary cellular injury occurs during the ischemic phase, while secondary damage predominantly arises during reperfusion. The initial ischemia establishes a highly toxic molecular environment, further exacerbated by the restored blood flow carrying these toxins into the brain tissue, resulting in a reformed microenvironment. Acidosis, a common feature of ischemia, emerges as a deleterious mechanism impacting neurons. The deprivation of oxygen and glucose during ischemia shifts glucose metabolism from aerobic oxidation to anaerobic glycolysis. This shift leads to a decline in pH due to the accumulation of glycolysis byproducts (8). Acidosis-induced injury not only results in neuronal death but also worsens the course of ischemia and reperfusion (9). Acid-sensing ion channels 1 (ASIC1) act as sensitive sentinels of tissue acidosis and are expressed in mammalian central and peripheral nervous system neurons. Initially, it was believed that the pathological activation of ASIC1-mediated acidosis induced neuronal injury and cell death through processes involving calcium (Ca2+) influx–mediated toxicity, receptor-interacting protein kinase 1 (RIPK1)-mediated necroptosis, or apoptosis (10–12). However, recent research indicates that disrupting ASIC1 through genetic ablation or selective pharmacological inhibition can confer protection against ischemia-reperfusion injuries, including cerebral stroke and myocardial infarction (8–13). Notably, both genetic ablation and pharmacological inhibition of ASIC1 have been found to reduce neuronal death following ischemic stroke in rodent models. These findings highlight the critical role of ASIC1 in mediating acidosis-induced neuronal injury and offer a promising target for therapeutic interventions in ischemia-reperfusion injuries, presenting potential avenues for mitigating the devastating impact of conditions like cerebral stroke and myocardial infarction.

We purified exosomes containing specific miRNA families from pluripotent stem cell–derived induced mesenchymal stem cells (iMSCs). These iMSC-derived exosomes demonstrated a dose-dependent protective efficacy in oxygen-glucose deprivation (OGD) neurons, effectively ameliorating neuronal death. We conducted RNA-seq to gain insights into the underlying mechanisms, which revealed a notable rewiring of the neuron transcriptome upon adding iMSC-derived exosomes. Subsequent small RNA-seq of the iMSC-derived exosomes identified ten prominent miRNA families. Our investigation identified a neuron-specific expression pattern of *Asic1* in the brain, with elevated ASIC1 levels directly indicating early cerebral ischemia-reperfusion damage. Through extensive analysis, we identified a miRNA cocktail composed of four miRNA families from the iMSC-derived exosomes that have the potential to target ASIC1.

Further validation experiments revealed that Hsa-mir-125b-5p, one of the four miRNA families, exhibited potent efficacy in rescuing neuronal death and promoting neuronal function. This effect was achieved through its selective suppression of *Asic1 in vitro* and *in vivo*. These findings provide critical evidence for the therapeutic potential of the specific miRNA content in iMSC-derived exosomes, particularly Hsa-mir-125b-5p, in mitigating cerebral ischemia-reperfusion damage by targeting *Asic1*. This research paves the way for the development of novel and targeted therapeutic strategies for treating ischemic stroke and other related neurological disorders.

Results

iMSC exosome purification and characterization

Cell culture supernatants from iMSCs at passages 3 and 5 were harvested for exosome purification after 48 h of cultivation in a xeno-free medium once cell confluency reached 80 to 90%. The morphology of the pre-enriched exosomes was examined using transmission electron microscopy, revealing typical bilayer membrane vesicles (Fig. 1A). Nanoparticle tracking analysis was performed, indicating a median exosome diameter of 102.1 nm (n = 3) (Fig. 1B). Flow cytometry assays confirmed the expression of specific exosomal markers CD63 and CD9 in the purified exosomes (Fig. 1C). To verify further the specific markers of EV, we identified a significant presence of TSG101, CD81, and syntenin. Concurrently, HSP90 and calnexin (14) were found to be scarcely detectable in EV derived from iMSC (Fig. 1D).

To explore the miRNA profile of iMSCs, small RNA-seq was conducted (Fig. 1E). Given the significant variability in the miRNA content among exosomes derived from MSCs of different origins (15–18) (Fig. S2B), we aimed to assess the consistency and stability of miRNA contents in iMSC-derived exosomes. Our analysis showed that the miRNA components and expression levels were consistent across different iMSC batches, indicating a reliable quality of exosomes produced by iMSCs (Fig. 1F). In total, 476 distinct miRNAs were identified, classified into 355 miRNA families (Fig. 1G).

iMSC-exosome alleviates OGD-induced neuronal death in a dose-dependent manner

To explore the ability of exosomes to transport internal materials into neuronal cytoplasm, we carried out a study examining the interaction between neurons and exosomes derived from iMSCs. We prelabeled iMSC exosomes with the red-fluorescent dye PKH26 and then cocultured them with neurons for 24 h. The detection of red fluorescence inside the neuronal cytoplasm confirmed the neurons' direct absorption of the exosomes (Fig. 2A).
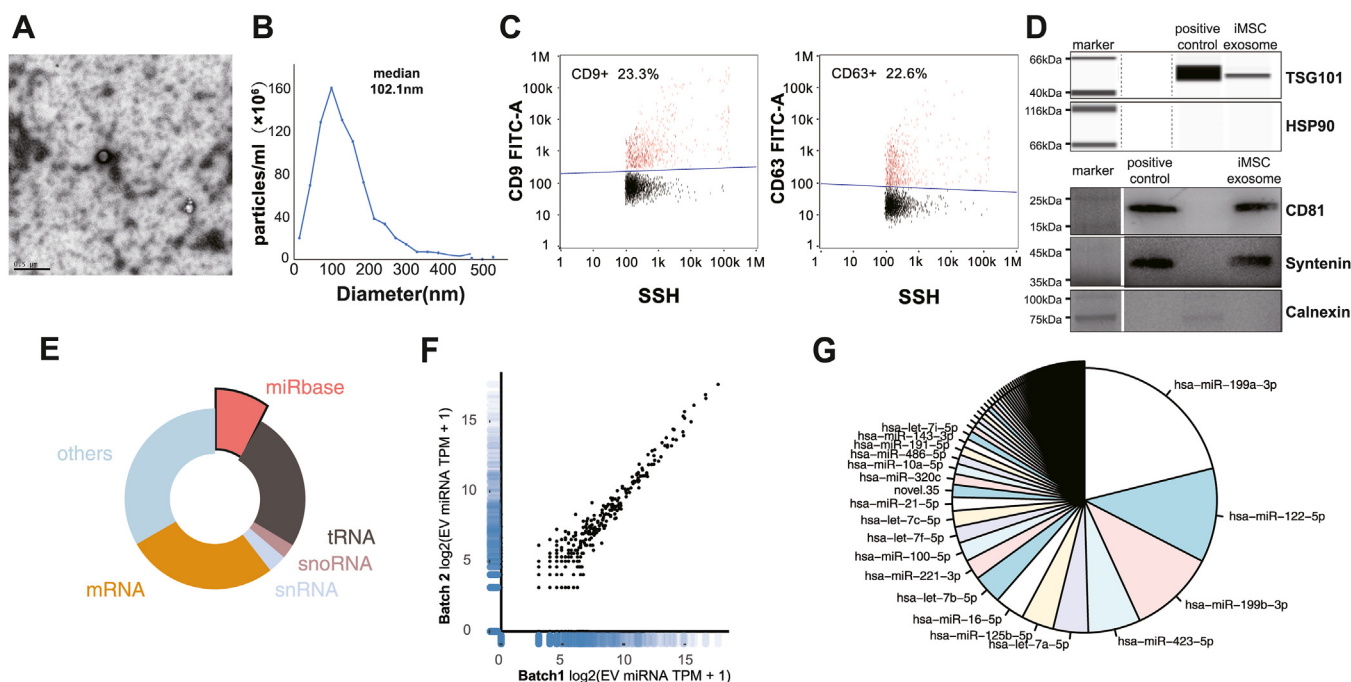
Figure 1. iMSC exosome and miRNA contents characterization. *A*, transmission electron microscopy images of iMSC exosomes. The scale length 0.5 μm. *B*, nanoparticle tracking analysis (NTA) of iMSC exosome size and particle concentration. The median diameter of exosome particles was 102.1 nm. The absolute count of exosome particles was determined and shown as particles/ml. *C*, flow cytometric analysis of the exosome marker CD63 and CD9 expression. *D*, Western blot of markers TSG101, HSP90, CD81, syntenin, and calnexin expression in iMSC-derived exosomes. *Dashed line* indicate the splice position of Western blot image. *E*, the *pie chart* shows the percentage of each RNA category within iMSC exosome small RNA-seq results. miRNA registered in miRBase is shown in *red color*. *F*, the scatter plot demonstrates the correlation of miRNA contents in two iMSC exosome batches. *x*-axis and *y*-axis indicate the log2 value of TPM +1 of each miRNA. *G*, the *pie chart* shows the percentage of miRNAs within the iMSC exosome. iMSC, induced mesenchymal stem cell; TPM, transcripts per million.

Following the demonstration that exosomes can effectively deliver materials into neurons, we investigated their potential to protect neurons under OGD stress. To simulate the ischemia-reperfusion scenario *in vitro*, E16 rat cortical neurons, after being cultured for 10 to 12 days, were subjected to 1.5 h of OGD stress (Fig. 2B). This was followed by 24 h of glucose and oxygen reperfusion, conducted with or without the addition of iMSC exosomes. The neurons were stained with propidium iodide (PI) to identify dead cells and Hoechst 33342 to mark all cells (Fig. 2B). Under OGD stress, the neuron death ratio soared to 42.4% (ratio of PI-positive to Hoechst 33342-positive cells), significantly surpassing the 2.56% death ratio seen in the control group not subjected to OGD stress (Fig. 2, C and D). This increase signalled reperfusion injury upon reintroducing glucose and oxygen to the cultured neurons. Assessing the therapeutic potential of iMSC exosomes, we introduced concentration gradients of exosomes into the culture medium during the reperfusion phase. The neuron death rate consistently decreased in a dose-responsive manner upon exosome treatment (Fig. 2D). Notably, the administration of iMSC exosomes significantly lowered the neuron death ratio to 37.4% (t(df) = 1.35, $p = 0.2257$), 32.9% (t(df) = 2.597, $p = 0.0408$), 24.6% ($p = 0.0286$), and 25.8% (t(df) = 3.0308, $p = 0.0229$) at concentrations of 10^7, 10^8, 10^9, and 10^{10} particles/ml, respectively ($p < 0.05$). Meanwhile, OGD also significantly reduced neurite outgrowth (Fig. 2E)., which was rescued by the delivery of iMSC-derived exosomes in a dose-dependent manner(Fig. 2F). This finding underscores

the beneficial impact of iMSC-derived exosomes on neurons experiencing OGD stress.

Building upon these encouraging findings, we conducted a detailed investigation into the alterations in gene expression within neurons subjected to OGD stress, as well as the changes in the transcriptome following the administration of exosomes derived from iMSC. The following in-depth analysis aims to elucidate the molecular underpinnings contributing to the therapeutic efficacy of iMSC exosomes in addressing neuronal injuries caused by OGD.

iMSC exosome rescued OGD-damaged neurons *via* transcriptome rewiring

To verify the enhanced survival of neurons subjected to OGD stress following treatment with iMSC exosomes, we hypothesized that a significant reconfiguration of the transcriptome occurs in neurons responding to OGD stress. This reconfiguration entails dynamic and complex changes in gene expression patterns upon the delivery of iMSC exosomes. To explore this hypothesis, we conducted RNA-seq on control neurons and neurons under OGD stress (Fig. 3A). We then quantified the RNA abundance in neurons experiencing OGD stress 24 h posttreatment with iMSC exosomes.

Concentrating on neurons damaged by OGD, we detected a widespread transformation in the transcriptome. Specifically, 7626 genes exhibited differential expression compared to control neurons (Fig. 3B). These genes were implicated in a
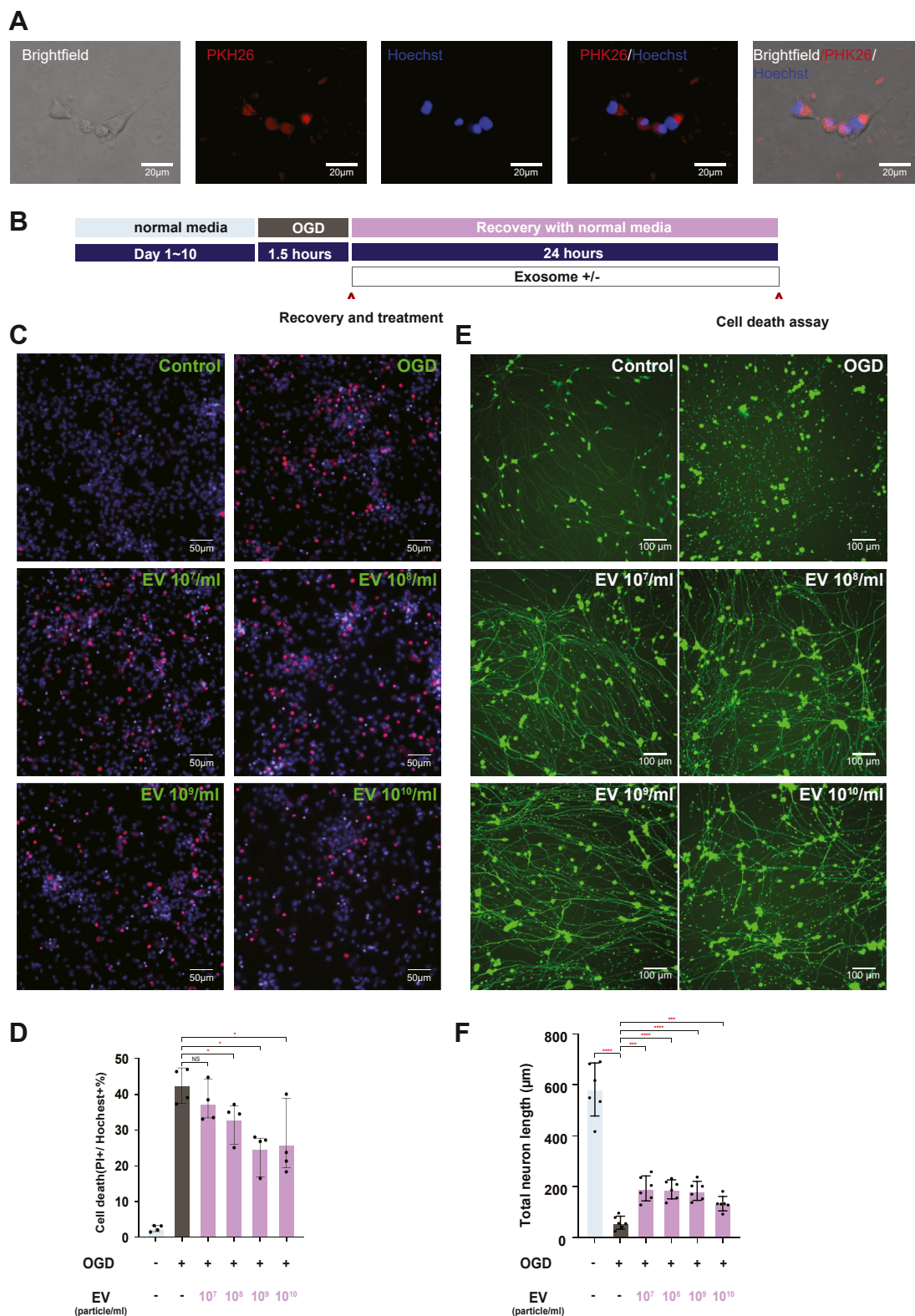
Figure 2. iMSC exosome alleviates oxygen and glucose deprivation–induced neuronal cell death in a dose-dependent manner. *A*, iMSC-exosome labeled with a red fluorescent dye PKH26 enriched in cultured rat cortical neuronal cytoplasm after 24 h of coculture. *B*, the experimental diagram to evaluate the effect of iMSC exosome against neuron OGD stress. *C*, representative images of PI and Hochest 33342 staining of cultured cortical neurons grow under control or OGD for 1.5 h and then are allowed to the standard culture medium for 24 h with different doses of iMSC exosome. The scale bar represents 50 μm. *D*, summary of PI-positive cells normalized to the total cell number determined by Hoechst staining. PI-positive ratio significantly decreases from 42.4% in OGD with the saline group control to 37.4%, 32.9%, 24.6%, and 25.8% in OGD with 10^8, 10^9, and 10^{10} iMSC exosome particles/ml. Sample size. N = 4. Comparison between samples was tested with unpaired *t* test. *E*, representative images of staining of cultured cortical neurons grow under control or OGD for 1.5 h and then are allowed to the standard culture medium for 24 h with different doses of iMSC exosome. The scale bar represents 100 μm. *F*, summary of total neurite length. Comparison between samples was tested with unpaired *t* test. Sample size N = 6. iMSC, induced mesenchymal stem cell; OGD, oxygen-glucose deprivation; PI, propidium iodide; TPM, transcripts per million.
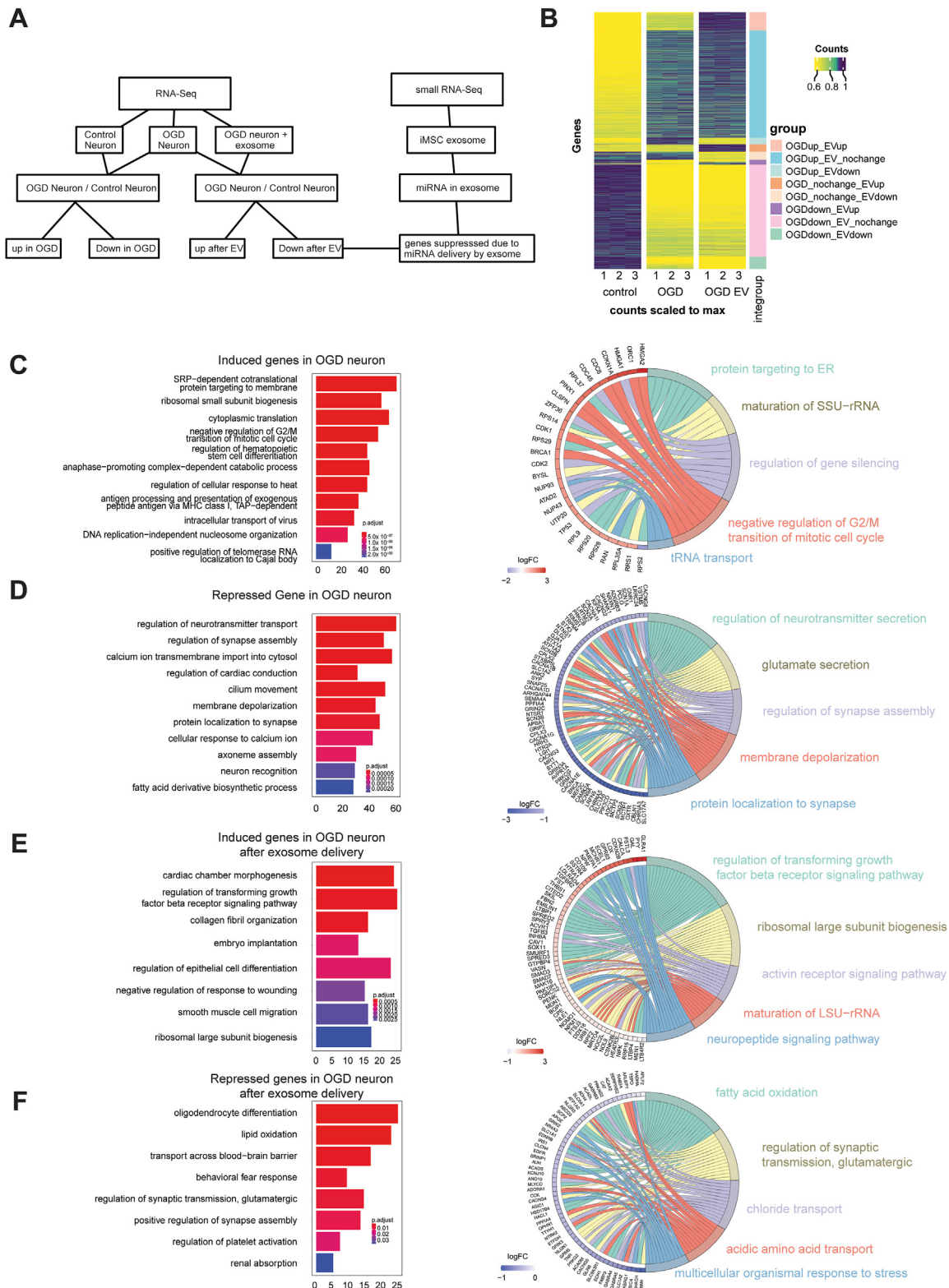
Figure 3. iMSC exosome rescued OGD-damaged neuron *via* transcriptome rewiring. *A*, the data analysis diagram to evaluate (1) transcriptome change in control, OGD-stressed neuron before and after iMSC exosome delivery; (2) miRNA contents within iMSC exosomes; (3) the potential mRNA suppressed by miRNA within exosome. *B*, heat map of variable genes of control neuron, OGD-stressed neuron, and exosome-rescued neuron. Heat map intensity represents relative RNA abundance for each replicate under different conditions. Gene intensity is normalized by maximum mRNA abundance across all treatments. *Yellow* indicates low expression, while *blue* indicates high RNA abundance. The *right-most column* shows gene categories according to gene expression patterns under different conditions. *C*, *left* barplot shows GO enrichment analysis of induced neutron response gene to OGD stress. On the *right side*, we demonstrate the enriched GO pathways and the differentially expressed genes induced by OGD stress in these pathways. *D*, *left* barplot shows GO enrichment analysis of suppressed neutron response gene to OGD stress. On the *right side*, we demonstrate the enriched GO pathways and the differentially expressed genes induced by OGD stress in these pathways. *E*, *left* barplot shows GO enrichment analysis of induced genes in OGD-stressed neutron after

range of cellular functions, such as cytoplasmic translation and the modulation of neurotransmitter receptor activity (Fig. S1A). Among these, 3780 genes were upregulated under OGD stress (fold-change > 1.2, p-adj < 0.00001), including genes involved in the negative regulation of the G2/M transition of the mitotic cell cycle and DNA replication–independent nucleosome assembly (Fig. 3C). Conversely, 3846 genes were downregulated in response to OGD stress (fold-change <1/1.2, p-adj < 0.00001), primarily associated with the regulation of neurotransmitter transport, synapse formation, and membrane depolarization (Fig. 3D).

Advancing our investigation to neurons rescued by iMSC exosomes after experiencing OGD stress, we observed a significant influence of iMSC exosomes on the gene expression profiles of OGD-affected neurons. Post delivery of iMSC exosomes, there was an upregulation of 961 genes (fold-change >1.2, p-adj < 0.00001) and a downregulation of 778 genes (fold-change < 1/1.2, p-adj < 0.00001) compared to OGD-stressed neurons that did not receive exosome treatment(Fig. 3B).

To understand how iMSC exosomes influence biological processes and potentially alter the pathological trajectory of ischemia-reperfusion injuries, we delved into the analysis of both upregulated and downregulated genes. This examination unveiled several biological processes being modulated, including fatty acid oxidation, the regulation of the transforming growth factor signaling pathway, cellular responses to acidic conditions, and the regulation of neuron projection (Fig. S1B). Subsequently, we concentrated on the specific genes induced or repressed after administering iMSC exosomes. The upregulated genes primarily facilitated the regulation of the transforming growth factor beta receptor signaling pathway and the biogenesis of the ribosomal large subunit (Fig. 3E). In contrast, the downregulated genes post-iMSC exosome treatment was linked to the regulation of synaptic transmission, glutamatergic activity, and lipid oxidation (Fig. 3F).

Our investigation specifically targeted biological processes related to neuronal death in the context of the comprehensive transcriptome changes prompted by the delivery of iMSC exosomes. A notable finding was the enhanced cellular response to acidic chemicals, echoing the phenomenon of tissue acidosis in ischemic conditions—a critical metabolic marker signaling the progression of injury in cerebral ischemia. We focused on genes activated by iMSC exosome treatment that played roles in cellular responses to acidic conditions and discovered that *Asic1*, an essential gene associated with acid-otoxicity, was significantly downregulated following the administration of iMSC exosomes to neurons experiencing OGD stress. Prior research has indicated that ASIC1 activation during tissue acidosis directly contributes to the deterioration of neurological function following cerebral ischemic stroke

(8, 19). Consequently, we delved deeper into identifying specific components encapsulated within iMSC exosomes that could inhibit *Asic1* expression.

Asic1 *expression in neuroblasts indicates early-phase reperfusion damage in cerebral stroke*

The bulk RNA-seq analysis revealed an upregulation of Asic1 in response to reperfusion damage. To investigate the specific cell types contributing to this elevation, we focused on the expression of *Asic1* in various cell types within cerebral tissues (20) (Fig. 4A). Among these cell types, neuroblasts exhibited a clear and significant expression of *Asic1* (Fig. 4B). Notably, the expression of *Asic1* was observed in neuroblasts both in normal brains and in brains subjected to reperfusion damage (Fig. 4C). In contrast, no evident *Asic1* expression was detected in microglial, astrocyte, oligodendrocyte, or endothelial cells (Fig. 4D).

Moreover, temporal analysis of *Asic1* expression in neuroblasts within the context of the middle cerebral artery occlusion (MCAO) mouse model unveiled compelling results. Specifically, an increase in *Asic1* expression was predominantly noted in the initial phase of reperfusion injury, precisely on the first day following MCAO induction (Fig. 4C). The proportion of neuroblasts expressing *Asic1* was significantly elevated during this early phase of ischemia-reperfusion injury. However, the upregulation of *Asic1* expression saw a decline in the subsequent stages of reperfusion, namely on the third and seventh days post-MCAO (Fig. 4C). These observations strongly indicate that *Asic1* could act as a valuable biomarker for early-stage neuronal damage in the context of cerebral stroke, especially during the reperfusion interval.

iMSC exosome–encapsulated miRNA suppresses neuronal death mediator Asic1

Exosomes are recognized for their capacity to transport diverse contents, including lipids, carbohydrates, RNA, and proteins, from donor to recipient cells. This process plays a crucial role in modulating cellular functions by repressing specific target genes (21). Based on this understanding, we hypothesized that exosomes derived from iMSC might contain a variety of miRNAs capable of inhibiting cell death signals in neurons subjected to OGD stress.

To explore the miRNA composition of exosomes derived from iMSC, we conducted small RNA-seq. We identified 476 distinct miRNAs (Fig. 1F), classified into 355 miRNA families according to miRBase release 22.1. Our analysis focused on the top ten miRNA families—miR-199-3p, let-7-5p/98-5p, miR-122-5p, miR-423-5p, miR-125-5p, miR-15-5p/16-5p/195-5p/424-5p/497-5p, miR-99-5p/100-5p, miR-221-3p/222-3p, miR-320, and miR-21-5p/590-5p—which together accounted for 82.3% of the total known miRNA content as per miRBase

---

iMSC exosome treatment. On the *right side*, we demonstrate the enriched pathways and also the differentially expressed genes in iMSC exosome-rescued neurons under OGD stress in these pathways. *F, left* barplot shows GO enrichment analysis of suppressed genes in OGD stressed neutron after iMSC exosome treatment. On the *right side*, we demonstrate the enriched pathways and the differentially expressed genes in IMSC exosome-rescued neurons under OGD stress in these pathways. GO, Gene Ontology; iMSC, induced mesenchymal stem cell; MSC, mesenchymal stem cell; OGD, oxygen-glucose deprivation.
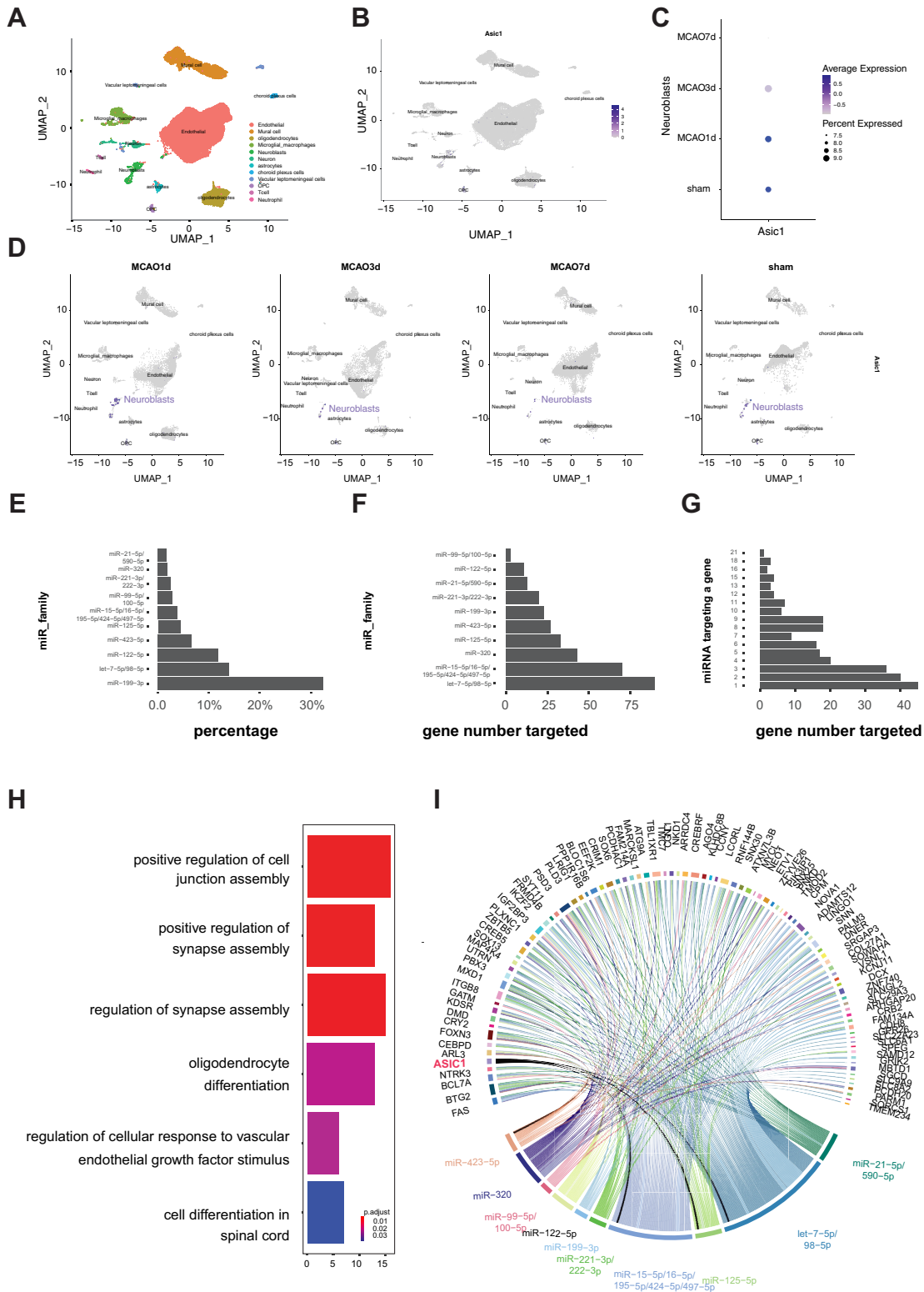
Figure 4. iMSC exosome–encapsulated miRNA cocktail suppresses neuronal death initiator ASIC1. *A*, reanalyzing of the single-cell data in Sham and OGD day 1, day 3, and day 7 mice. Cell population with different identities is labeled with the corresponding color indicated in legends. *B*, dot plot indicates cell type–specific expression of *Asic1*. *Dot size* indicates the percentage of cells that are expressed. *Blue saturation* indicates the average expression of *Asic1* within a cell population. *C*, dot plot indicates *Asic1* expression in neurons in sham, MCAO day 1, 3, and 7 mice. *Dot size* indicates the percentage of cells that are expressed. *Blue saturation* indicates the average expression of Asic1 within a cell population. *D*, feature indicates Asic1 expression in each cell type in sham, MCAO day 1, day 3, and day 7 mice. *E*, the *bar chart* shows the percentage of each top 10 miR families occupied. *F*, the *bar chart* shows the gene number of the top 10 miR families targeted. *G*, the *bar chart* shows the gene numbers *x*-axis) that could be simultaneously targeted by multiple numbers of miRNAs *y*-axis. *H*, bar plot of GO enrichment analysis of genes predicted to be targets of top 10 miRNA families within iMSC exosome and repressed after

release 22.1 (Fig. 4, *E–G*). We then examined the genes targeted by these miRNA families and those downregulated following iMSC exosome delivery, as revealed by RNA-seq data. This analysis highlighted a subset of 249 genes, downregulated by miRNAs in iMSC exosomes, implicated in regulating neuronal synaptic plasticity, cellular response to acidic conditions, and calcium ion import across the plasma membrane (Fig. 4*H*). Specifically, we scrutinized miRNA families with potential targeting capacity for Asic1 (Fig. 4*I*), a critical mediator of acidosis-induced neuronal death. We noted that iMSC exosomes could mitigate neuronal death induced by ischemia-reperfusion injuries. Among these, four miRNA families—miR-125b-5p, let-7-5p/98-5p, miR-15-5p/16-5p/195-5p/424-5p/497-5p, and miR-423-5p (Fig. 4*I*), were notably enriched, representing 37.8% of the total miRNA abundance in iMSC-derived exosomes, as per miRBase release 22.1. Our objective was to ascertain whether these four miRNA families could effectively downregulate Asic1 expression and thus facilitate the condition of neurons stressed by OGD.

iMSC exosome rescue the neuronal cell death via miR-125b-5p mediate Asic1 suppression in vitro

In vitro, we evaluated the neuroprotective effect of the miRNA families mentioned above on neurons subjected to OGD stress (Fig. 5*A*). The introduction of hsa-miR-125b-5p mimics markedly reduced neuronal death, with the ratio of PI-positive cells decreasing to 25.1% (t(df) = 3.132, p = 0.0351), an outcome comparable to that achieved through the administration of iMSC-derived exosomes, which resulted in a cell death ratio of 21.74% (t(df) = 2.967, p = 0.0413) (Fig. 5*B*). Conversely, the administration of the other three miRNA mimics—hsa-miR-16-5p (p > 0.999), hsa-miR-143-3p (t(df) = 1.657, p = 0.1728), and hsa-miR-423-5p (t(df) = 0.8456, p = 0.4454)—did not yield a significant protective effect (Fig. 5*B*). These findings highlight hsa-miR-125b-5p as the critical component within iMSC exosomes that is instrumental in the rescue of neurons from OGD-induced stress.

To corroborate the role of hsa-miR-125b-5p in downregulating *Asic1* expression and facilitating neuroprotection, we conducted Western blot analyses on neurons damaged by OGD. A significant reduction in ASIC1 protein levels was observed following the administration of both iMSC exosomes and hsa-miR-125b-5p mimics (Figs. 5, *C* and *D*, S3). This suppression of ASIC1 protein by hsa-miR-125b-5p delivery likely underlies the neuroprotective mechanism of iMSC exosomes within the context of cerebral ischemia-reperfusion injury.

iMSC exosomes rescue neuronal death via suppression of necroptosis initiated by ASIC1

In light of the elevated ASIC1 levels observed in neurons injured by cerebral ischemia-reperfusion, we aimed to identify the specific molecular phenotype of cell death induced. Prior studies have hinted at a connection between increased ASIC1 levels and necroptosis (11). Indeed, during the reperfusion phase, we noted a rise in the expression of phosphorylated mixed lineage kinase domain–like protein (MLKL) (Figs. 5, *E* and *F*, S3), a pivotal agent in plasma membrane disruption and a key executor of necroptosis. Furthermore, RIPK1, a necroptosis initiator, was also found to accumulate in neurons affected by reperfusion injury (Figs. 5, *E* and *F*, S3).

Given the activation and accumulation of necroptosis initiators and executors following reperfusion damage, we explored the potential of iMSC-derived exosomes to reverse this cell death pathway. After administering iMSC exosomes to neurons damaged by reperfusion, we assessed the activity of crucial necroptosis components. Remarkably, compared to untreated reperfusion-injured neurons, a significant decrease in the levels of activated RIPK1 and MLKL was observed following exosome treatment, indicating a neuroprotective effect of iMSC-derived exosomes against necroptosis-induced neuronal death. To further substantiate the contribution of exosomal contents, specifically hsa-mir-125b-5p, to this protective mechanism, we introduced hsa-mir-125b-5p mimics. These mimics exhibited protective outcomes similar to those of iMSC exosomes by downregulating ASIC1 and phosphorylated RIPK1 (Figs. 5, *E* and *F*, S3).

Moreover, a marked reduction in p-MLKL levels was evident upon the administration of hsa-mir-125b-5p mimics (Figs. 5, *E* and *F*, S3), reinforcing the notion that iMSC-derived exosomes mitigate necroptosis in neurons. Both the iMSC exosomes and their active component, hsa-mir-125b-5p, play crucial roles in reducing ASIC1 and its associated activated RIPK1 levels, as well as in the decline of the final necroptosis executor, p-MLKL, underscoring their potential in neuronal protection by mitigating necroptosis.

iMSC exosomes alleviate postischemic injury in rat MCAO models in vivo

Our research was aimed at exploring the *in vivo* effects of hsa-miR-125b-5p encapsulated within exosomes (Fig. 6*A*). In the group of rats subjected to MCAO, we observed pronounced neurological deficits. Triphenyltetrazolium chloride (TTC) staining disclosed a significant infarction volume of 36 ± 2% in the cerebral tissue of MCAO rats compared to the sham-operated group (Fig. 6, *B* and *C*). The administration of exosomes derived from iMSCs diminished the infarction volume to 32 ± 7% (Fig. 6, *B* and *C*). Notably, the sole administration of hsa-miR-125b-5p mimics markedly enhanced resistance to cerebral injury, reducing the infarction volume to 28 ± 6% (Fig. 6*B*), which mirrors the therapeutic efficacy observed with the complete exosome delivery. Neurological assessments further corroborated this level of recovery following treatment with hsa-miR-125b-5p mimics (Fig. 6*D*).

iMSC exosome treatment. *I*, circos plot demonstrates the most abundant top 10 miR families within iMSC EV and their corresponding target genes that were repressed in OGD-damaged neurons after iMSC exosome treatment, which is validated by RNA-seq. *Asic1*, acid-sensing ion channel 1; GO, Gene Ontology; iMSC, induced mesenchymal stem cell; MCAO, middle cerebral artery occlusion; OGD, oxygen-glucose deprivation.
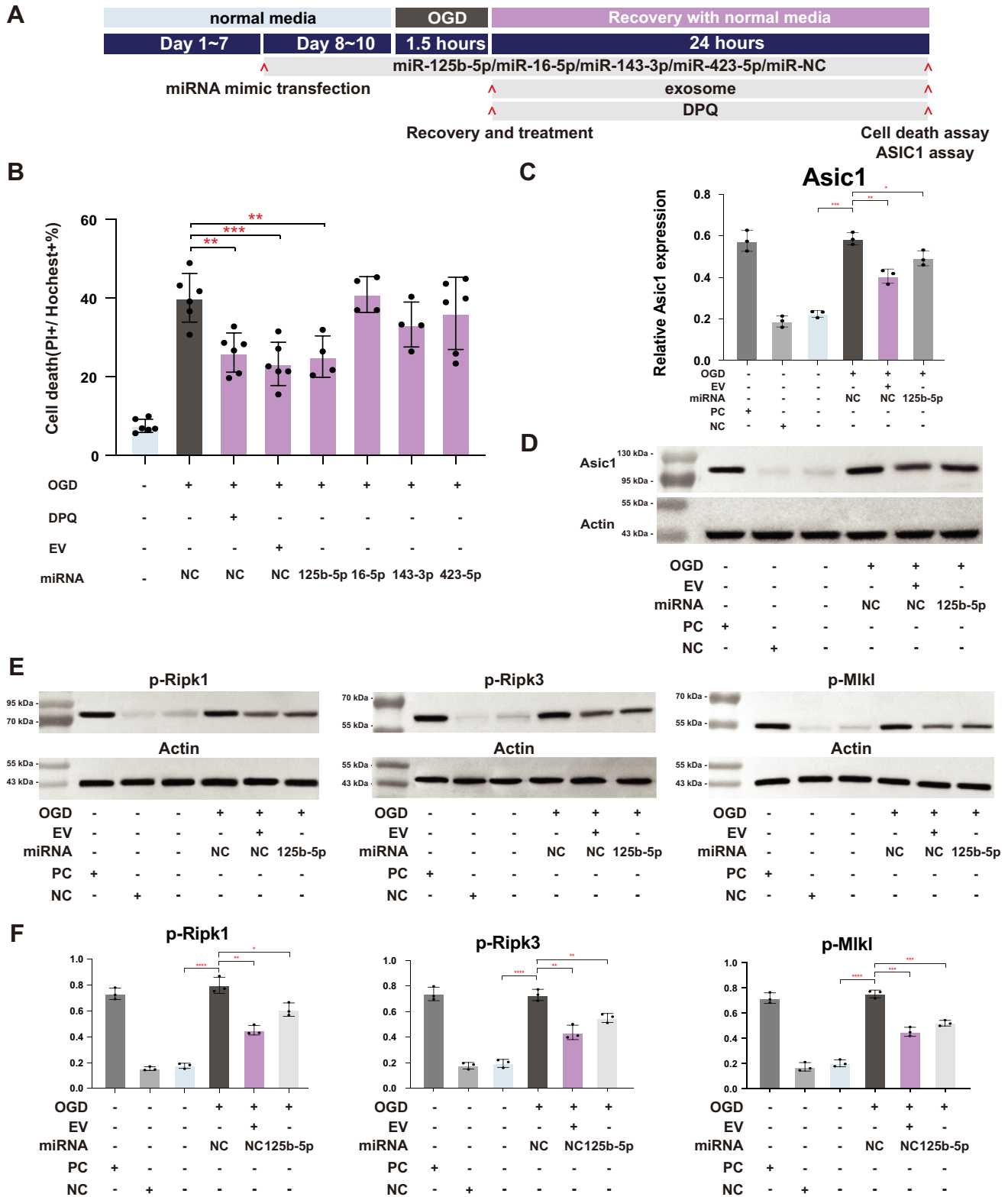
Figure 5. iMSC exosome rescues the neuronal cell death *via* hsa-miR-125b-5p mediate *Asic1* suppression. *A*, the experimental diagram to validate the effect of four specific miRNA encapsulated by iMSC exosome against neuron OGD stress. *B*, cell death rate under the condition: control, OGD, OGD + DPQ, OGD + exosome, OGD + hsa-miR-423-5p mimic, (sample size N = 6). OGD + hsa-miR-125b-5p mimic, OGD + hsa-miR-16-5p mimic, OGD + hsa-miR-143-3p mimic, sample size N = 4. *C*, Western blot quantification. The iMSC exosome and hsa-miR-125b-5p mimic suppressed ASIC1 protein expression. Comparison between samples was tested with unpaired *t* test, (sample size N = 3). *D*, Western blot. The iMSC exosome and hsa-miR-125b-5p mimic suppressed ASIC1 protein expression. *E*, Western blot. The iMSC exosome and hsa-miR-125b-5p mimic affect phospho-RIPK1, phospho-RIPK3, and phospho-MLKL protein expression in OGD-stressed neurons. *F*, quantification of Western blot for phospho-RIPK1, phospho-RIPK3, and phospho-MLKL protein expression. Comparison between samples was tested with unpaired *t* test, (sample size N = 3). *Asic1*, acid-sensing ion channel 1; iMSC, induced mesenchymal stem cell; MLKL, mixed lineage kinase domain–like protein; OGD, oxygen-glucose deprivation; RIPK, receptor-interacting protein kinase.
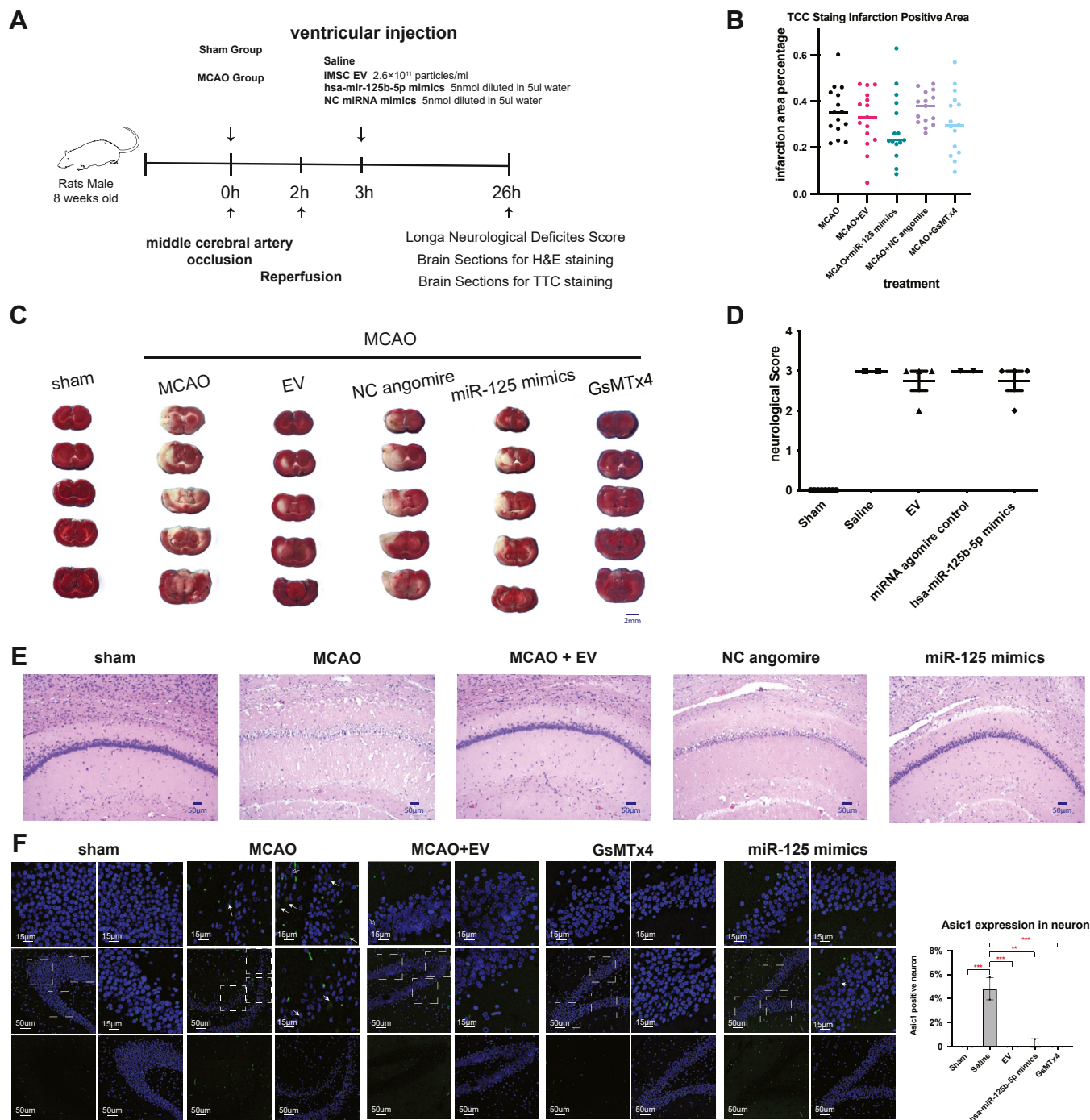
Figure 6. iMSC neuroprotective effects of iMSC-derived exosome on cerebral infarction. *A*, design and timeline of the animal experimental procedure. Male rats were subjected to sham and MCAO surgery followed by an i.v. injection with hsa-miR-125b-5p mimics, NC microRNA mimics control, EV, saline, or GsMTx4. After 24 h, rats were subject to neurological scoring tests, and brains were collected for histological processing. *B*, TTC stained serial coronal rat brain sections of the cerebral infarct. *C*, iMSC exosome reduced infarct volume significantly. Delivery of hsa-mir-125b-5p mimics reached a comparable therapeutic effect as MSC exosome delivery. The *y*-axis indicates the percentage of infarction volume. Slide sample size N = 15. The scale bar represents 2 mm. *D*, the neurological score of sham group and MCAO before and after EV and hsa-mir-125b-5p treatment. N = 4. *E*, post cerebral ischemia-reperfusion H&E staining in the rat hippocampus. Magnification, × 400. In the MACO model, necrotic cells, shrunken nuclei, and brain swelling were observed in the whole hippocampal region. iMSC exosome delivery restored cell morphology. Hsa-mir-125b-5p delivery also improved the cell morphology, similar to the iMSC exosome. The scale bar represents 50 μm. *F*, post cerebral ischemia-reperfusion ASIC1 immunofluorescent staining in the rat hippocampus. The *white arrow* indicates the detected ASIC1 expression in neurons. Comparison between samples was tested with unpaired *t* test. ASIC1, acid-sensing ion channel 1; EV, extracellular vesicle; iMSC, induced mesenchymal stem cell; MCAO, middle cerebral artery occlusion; MSC, mesenchymal stem cell; OGD, oxygen-glucose deprivation; TCC, triphenyltetrazolium chloride.

Subsequently, our investigation extended to the histological recovery. H&E staining of brain tissue unaffected by ischemia showcased the preservation of characteristic hippocampal and cortical structures, with neurons displaying standard morphology and clearly visible nucleoli. Conversely, the MCAO model illustrated the repercussions of ischemia and
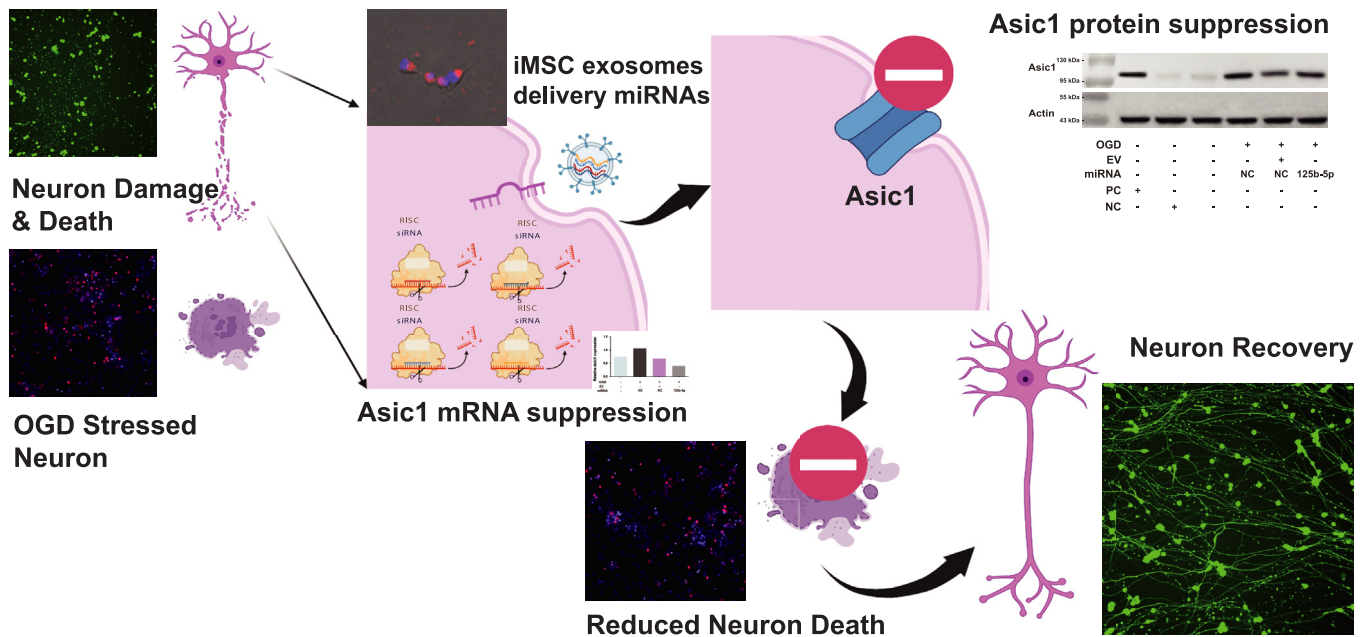
Figure 7. iMSC exosome therapeutic effect against cerebral ischemic stroke by suppressing Asic1 *via* delivery of hsa-miR-125b-5p. Created with BioRender.com under publication agreement number: YW247PMNM4. iMSC, induced mesenchymal stem cell.

reperfusion injury, evidenced by a reduction in neuron numbers and compromised neuronal morphology (Fig. 6E). Nevertheless, the application of MSC-derived exosomes facilitated the restoration of neuronal morphology. Further analysis revealed that this neuroprotective effect could be attributed predominantly to hsa-miR-125b-5p. Indeed, the administration of hsa-miR-125b-5p mimics significantly ameliorated neuron integrity when compared to the negative control (NC) group (Fig. 6E), highlighting the therapeutic potential of hsa-miR-125b-5p delivered *via* MSC-derived exosomes (Fig. 7).

In this study utilising the MCAO model, we further examined whether ischemic brain injury *in vivo* leads to alterations in ASIC1 expression in neurons and whether treatments with iMSC-derived exosomes and hsa-mir-125b-5p could mitigate these changes. Compared to the sham control group, MCAO induced a significant increase in ASIC1 expression within the neurons of the dentate gyrus (Fig. 6F), with the proportion of ASIC1-positive neurons rising from 0% to 4.8% ($p = 0.0008$) (Fig. 6F). Treatment with iMSC exosomes and hsa-mir-125b-5p notably decreased the prevalence of ASIC1-positive neurons from 4.8% to approximately 0% to 0.2% ($p < 0.005$), without leading to any significant adverse side effects.

Discussion

EVs mediated miRNA communication plays a pivotal role in various diseases across multiple organs such as the breast (22), heart (23–27), and brain (25, 28), involving tumour occurrence, chemotherapy resistance (28), metastasis, ischemic stroke (24, 25), acute cellular cardiac rejection, and heart transplantation (27) and atherosclerosis (23). Under adverse conditions, miRNA signaling through EVs enhances the resilience of target cells, enabling tumor cells, for example, to

transform sensitive cells into resistant ones and remodel distant healthy organs to foster a tumor-friendly microenvironment (22). Similarly, the therapeutic potential of exosomes in treating cerebral ischemia has been demonstrated, yet the lack of precise mechanisms and targets hinders its translation into clinical applications. Our findings reveal that iMSC-derived exosomes can deliver a controlled mixture of miRNAs, particularly targeting the Asic1 protein to salvage neuronal death. We identified miR-125b-5p as a key active component and validated its neuroprotective function in an OGD model. Our results show that iMSC-derived exosomes restore the function of damaged neurons by targeting the Asic1 protein.

Exosomes originating from MSCs have shown promising results in reducing ischemia/reperfusion injury in various cell or animal models, including acute myocardial (29), renal (30) and brain ischemia-reperfusion models (31). Various tissues and cell types, including endothelial cells (23), macrophage (28), and fibroblast (24), are capable of secreting exosomes containing miRNAs, which facilitate cell communication through paracrine (28) and systemic circulation (32), thereby mediating biological effects. miRNAs within EVs exhibit dual roles; on the one hand, they possess pathogenic effects, and on the other hand, they hold significant clinical value for diagnosing (32) and treating diseases. Our study demonstrated that iMSC-exosomes effectively rescue neuronal death under OGD injury in a dose-dependent manner. mRNA sequencing data indicated significant changes in the mRNA expression of injured neurons after iMSC-exosome delivery. Gene ontology analysis of differentially expressed genes revealed an enrichment in the cellular response to acid chemicals. Notably, ASIC1, a critical mediator of acidosis during ischemic stroke, was significantly downregulated by iMSC-exosomes. ASIC1

activation in neurons can lead to cell death through various mechanisms, including calcium overload, regulation of mitochondrial permeability transition pores, and the initiation of necroptosis. Inhibiting *Asic1* through iMSC delivery could block these molecular events and alleviate neuronal cell death under OGD stress.

Exosomes have been shown to restore injured cell function by delivering miRNAs. To elucidate the potential therapeutic mechanism, it is essential to identify which specific miRNA or group of miRNAs encapsulated by exosomes is effective in neurons under OGD stress. In our study, we found that iMSC exosomes stably express around 400 kinds of miRNAs, and we focused on the top miRNA families, accounting for 82.3% of all miRNA content. Through prediction using different databases, we identified four miRNA families encapsulated by iMSC exosomes that could target *Asic1*. To validate the effectiveness of these miRNAs in rescuing OGD-induced neuronal death, we transfected hsa-miR-125b-5p, hsa-miR-16-5P, and hsa-miR-423-5p mimics individually and found that hsa-miR-125b-5p mimic transfection significantly suppressed ASIC1 protein levels and alleviated neuronal death. In conclusion, we propose that iMSC exosomes rescue OGD-injured neuronal death primarily by repressing ASIC1 through hsa-mir-125b-5p.

The clinical application of exosomes faces challenges related to product stability, including the consistency of exosome content from the same type of cells, heterogeneity in preparation procedures, lack of standardized quality control, and unclear mechanisms. The loading of miRNAs into exosomes is mediated by RNA-binding proteins through an ATP-dependent active process, selectively incorporating specific miRNAs into exosomes. This ensures the stability of miRNA components in EVs secreted by homogenous cells, as evidenced by the high correlation in our multiple biological replicates of small RNA-seq. To address potential variations in exosome quality, we employed pluripotent stem cell–derived cells with MSC characteristics to produce exosomes under a controlled process. By establishing a standardized cell bank, qualified iMSCs and exosomes could be produced consistently using pluripotent stem cells. We controlled the passage of cells and culture conditions, ensuring that iMSCs produce exosomes of stable quality and scalable production capacity. Furthermore, we characterized our iMSC exosomes from different batches, and the results from nanoparticle tracing, nanoparticle flow, and miRNA sequencing indicate that our differentiation protocol consistently produces exosomes with similar miRNA contents.

However, while we have demonstrated that EVs derived from iMSCs can rescue the morphology and functions of neurons stressed by OGD in both cell lines and animal models, further clinical studies are necessary to confirm their therapeutic effects in patients with cerebral stroke. Additionally, the dynamic changes in Asic1 expression in patients during the course of a stroke warrant further investigation.

In summary, our study demonstrates that exosomes derived from iMSCs could serve as a novel cytoprotective therapy for OGD by inhibiting acidosis initiated by ASIC1, and hsa-mir-125b-5p delivered by iMSC exosomes may play a crucial role in promoting neuronal survival.

Experimental procedures

MSC exosome purification and characterization

iMSC supernatant was kindly provided by Zephyrm Biotechnologies. To prepare cells for supernatant harvesting, human embryonic stem cell–derived iMSC (passage 5–8) was seeded at a density of 2×10^4 cells per cm^2 and cultured for 3 days until the confluence reached 60 to 70% (5×10^5/ml) in the serum-free medium. Before 48 h of iMSC exosome isolation, fresh medium was fed and maintained without medium change. iMSC exosome was purified with Total Exosome Isolation Kit (4484450 Thermo Fisher Scientific) according to the manufacturer's instructions. Briefly, cell media were centrifuged at 2000g for 30 min to remove cells and debris. The cell-free culture media were mixed with 0.5x volumes of isolation reagent and incubated at 2 °C to 8 °C overnight. Then, the mixture samples were centrifuged at 10,000g for 1 h from 2 °C to 8 °C. The collected exosomes were resuspended with PBS for characterization and downstream experiments.

Nanoparticle tracking analysis (ZetaView) analyzed the particle size and concentration. The morphology of the iMSC-exosome was observed by transmission electron microscopy (Joel JEM1230). Exosome surface markers CD63 and CD9 were analyzed by Flow NanoAnalyzer (nanoFCM software v 1.08) (https://www.nanofcm.cn).

Rat cortical neuron cell culture and OGD

Neurons for OGD were primarily cultured from gestational day 16 fetal rats as previously described (33). OGD was performed on day 10. Briefly, the standard neuron medium was washed two times and incubated in Dulbecco's Modified Eagle Medium with no glucose prebubbled with 95% N_2 and 5% CO_2 for 10 min to saturate. Then cultures were treated for 1.5 h in an OGD anaerobic chamber. The control group was cultured in normal conditions. A standard neuron culture medium with glucose was exchanged, and 74% N2/21% O2/5% CO2 was recovered. Exosomes at different concentrations (0, 10^8, 10^9, 10^{10} particles/ml) were added when shifted to normal conditions.

Neuron survival assay

Twenty-four hours after OGD recovery with or without iMSC-exosome administration, cultured neurons were stained with PI for labeling dead cells, and Hochest 33342 (molecular probes) for all cell nuclei. Survival assay was performed by counting PI-positive cells ratio *versus* Hoechst labeled cell nuclei under a high-content imaging system (Thermo Fisher Scientific CellInsight CX5). For normally distributed data, data were analyzed by ANOVA with the Student's *t* test for independent means. At least three independent experiments using four separate wells were performed for a minimum of 16,000 to 30,000 neurons counted for each data point.

Neurite outgrowth analysis

Analyses of neurite extension were performed on the CellInsight CX5 high-content screening platform. Random image fields were taken. Neurite length was determined by tracing the length of the longest neurite of differentiated cells using the Neurite Detection Assay module in Thermo Scientific HCS Studio: Cellomics Scan Version 6.6.1. The p value was calculated using the student t test.

RNA-seq experiment and library preparation

The total mRNA was extracted with RNeasy Micro Kit (74004 Qiagen) following the manufacturer's instructions for library construction. Qualified total RNA was purified by RNAClean XP kit (A6398.7, Beckman Coulter, Inc) and RNAase-Free Set (79254, QIAGEN). The sequencing library was prepared with VAHTS Universal V6 RNA-seq Library Prep Kit for Illumina (NR604-02, Vazyme) according to the manufacturer's instructions. Final library concentration was measured by Qubit dsDNA HS Assay Kit (Q32850, Invitrogen). The quality control of the library was performed using the Agilent Bioanalyzer 2100 system. Cluster generation was performed on the cBot Cluster Generation System (Illumina). The library was sequenced using Illumina Hiseq 2500 instrument with paired-end mode.

Exosome miRNA library preparation

Shanghai Biotechnology performed iMSC-exosome miRNA library construction and sequencing. miRNAs of iMSC exosomes were extracted using the mirVana miRNA Isolation Kit (AM1561) and qualified by Qubit 2.0. RNA integrity was analyzed by Agilent 2100 Bioanalyzer (Agilent Technologies Santa Clara) . Exosomal RNA from each sample was used for small RNA library construction. The final library was sequenced on the HiSeq2500 platform.

Processing and analysis of RNA-seq data

Samples were sequenced from 54.33 million reads to 64.34 million reads per sample, with 58.84 million reads as median. Three biological replicates were performed for each condition. Ribosome RNA percentage ranged from 0.05% to 0.11%, with a median value of 0.085%. Genome assembly and annotation data were downloaded from Ensembl database and annotation from the Ensembl database (ftp://ftp.ensembl.org/pub/release-83/fasta/rattus_norvegicus/dna/Rattus_norvegicus.Rnor_6.0.dna.toplevel.fa). The mapping rate ranged from 85.78% to 93.84% with median value of 93.41%. RNA-seq data quality was assessed by FastQC (https://www.bioinformatics.babraham.ac.uk/projects/fastqc/). Reads were preprocessed with Seqtk. The preprocessing includes the following: (1) removing the adaptor; (2) remove low-quality nucleotides (based on Q20) at the 3′end of the reads; (3) removing reads shorter than 25 nt after preprocessing; (4) removing known rRNA. Reads were then aligned with Hisat2 (34, 35) (version: 2.0.4), splicing mapping to rat genome reference (Rnor_6.0 from Ensembl database). Reads were summarized into gene expression values with Stringtie (18) (version: 1.3.0). Read counts were normalized with trimmed mean of M values (36) methods and then fragments per kilobase of exon model per million mapped reads values were calculated. Differential gene expression analysis was performed using the EdgeR (37).

Analysis of miRNA data

Samples were sequenced from 20.8 million reads to 25.4 million reads per sample, with 23.8 million reads as median. Three biological replicates were performed for each condition. Genome assembly and annotation data were downloaded from the Ensembl database. Raw reads were preprocessed with fastx (version:0.0.13) to (1) remove adaptor sequence, (2) remove low-quality nucleotide (Q10) from 3′end of reads, and 3) remove reads with length <10 bp, all reads were 18 to 40 nt selected reads. Preprocessed reads were aligned to reference genome GRCh38 with bowtie (38). miRNA counts were then further extracted based on the genomic position provided by miRbase (39). Extracted miRNA counts were normalized with the trimmed mean of M values method, and then the transcripts per million) value was calculated to compare samples. In predicted and validated miRNA target analysis, we used the multimir (40) and circlize (41) packages to plot the abundant top miRNA and their corresponding suppressed mRNA targets. The scientific calculations in this paper have been done on the HPS Cloud Platform of Shandong University.

miRNA mimic transfection

miRNA mimics and control were synthesized by Ribobio and transfected using a RiboFECT CP transfection kit(C10511-05 Ribobio). Briefly, 50 nM miRNA mimics were mixed with transfection reagent and incubated for 15 min at room temperature. The transfection mixture was added to cultured neurons without antibiotics in the medium. Medium change is not required. Seventy-two hours later, transfected neurons were used for OGD experiments.

Western blotting

Proteins (10 μg) extracted from neurons were diluted in a loading buffer, heated at 95 °C for 10 min, loaded onto 12% gels, electrophoresed at 180 V for 50 min, and transferred to membranes. After blocking with a blocking buffer for 60 min, the membranes were incubated with primary antibodies at 4 °C overnight and washed in 1× Tris-buffered saline, 0.1% Tween 20 Detergent (3 × 5 min). Then, the membranes were incubated with secondary antibodies at room temperature for 60 min, washed with 1× Tris-buffered saline, 0.1% Tween 20 Detergent, and exposed to a detection reagent for visualization. The images were acquired *via* Bio-Rad chemidoc system, and band intensities were quantified with ImageJ (https://imagej.net/ij/download.html). The antibody information was as follows: ASIC1 (Immunoway, YN5678, 1:500), β-ACTIN (Abmart, M20011, 1:2000), goat anti-rabbit IgG-horseradish peroxidase (Abmart, M21002, 1:5000), goat anti-mouse IgG horseradish peroxidase (Abmart, M21001, 1:5000), phospho-RIPK1 (Immunoway, YP1467), phospho-RIPK3 (Immunoway, YP1468), and phospho-MLKL (Immunoway, YP1244),

calnexin (Abcam ab10286), CD81 (Santa Cruz Biotechnology, INC sc-166028), HSP90 (Santa Cruz Biotechnology, INC sc-69703), syntenin-1 (C-3) (Santa Cruz Biotechnology, sc-515538), and TSG101 (HUABIO, ET1701-59). For ASIC1, p-RIPK1, p-RIPK3, and p-MLKL, L929 cells treated with zVAD (20 μM) for 1 h, and then TNF (10 ng/ml) for 6 h were used as a positive control. Meanwhile, healthy L929 cells were utilized as an NC.

GO, Kyoto Encyclopedia of Genes and Genomes analysis, and plotting

For Gene Ontology (GO) and Kyoto Encyclopedia of Genes and Genomes enrichment analysis, we used clusterprofiler (42). Enriched GO terms and pathways were plotted with R package enrichplot (https://github.com/YuLab-SMU/enrichplot) and GOplot (43).

Real-time PCR for mRNA and miRNA analysis

The total RNA was extracted using PureLink RNA Micro kit (12183016 Thermo Fisher Scientific). According to the manufacturer's protocol, complementary DNA was generated *via* SuperScript IV (18090050, Thermo Fisher Scientific) and Bulge-Loop miRNA qRT-PCR Starter Kit (C10211-1, Ribobio). Thereafter, real-time PCR was carried out using complementary DNA samples, and the $2^{-\Delta\Delta Ct}$ method was used to calculate the relative change in mRNA and miRNA expression after normalization to levels of GAPDH for mRNA and U6 small nuclear RNA for miRNA.

Statistics

Sample size calculation : In determining the appropriate sample size for our animal experiments, we conducted an *a priori* power analysis. Based on the anticipated effect size, the expected variability from previous studies, an alpha level of 0.05, and a desired power of 0.80, the optimal sample size was determined to be eight animals per group. Therefore, we used eight animals in each experimental group to ensure adequate statistical power and minimize the risk of type II errors. Randomization : Animals were randomly allocated to different experimental groups using a computer-generated random sequence. This randomization ensured that each animal had an equal chance of being assigned to any group, minimizing potential biases and confounding factors. A normality test : For the cell line experiment, we use the Shapiro–Wilk test for the normality test. For animal experiments, normality and variance homogeneity are assessed by the D'Agostino and Pearson test in Prism Graph 9.0 (https://www.graphpad-prism.cn). We have performed the Mann–Whitney test to compare groups that are not normally distributed. For groups that are normally distributed, we performed an unpaired *t* test. Data are displayed as median and interquartile range. (ns, $p < 0.10$; *$p < 0.05$; **$p < 0.01$; ***$p < 0.001$; and ****$p < 0.0001$).

Animal experiments

Adult male SD rats (220–250 g, 8 W) were purchased from Beijing HFK Bioscience. Animal experiments were carried out by the National Institutes of Health guide for the care and use of laboratory animals. The animal experiment protocol was examined and approved by the animal ethics committee of the Ethics Committee from Animal Care and Welfare Committee at Xuan Wu Hospital (XW-20210423-2). Four rats were hosted per cage.

As previously described, rat ischemia-reperfusion models were induced by MCAO surgery (44). Briefly, rats were anaesthetized with 3% pentobarbital sodium. The left common carotid artery, external carotid arteries and internal carotid artery were isolated and ligated. A monofilament nylon suture coated with silicon resin was inserted from the external carotid artery into the lumen of the internal carotid artery (time 0 h). Body temperature was maintained at 37 ± 0.5 °C through a thermostat-controlled heating pad. Reperfusion was initiated by the withdrawal of the monofilament after 120 min occlusion (time 2 h). The first set of MCAO rat models was administered saline and exosomes (2.6×10^{11} particles/ml) through ventricular injection. The second set of rats exposed to MCAO was administrated with hsa-mir-125b-5p mimics and miRNA NC control (5 nmol diluted in 5 ul water) (time 2 h), as well as 2 ng/kg (kg body weigth) GsMTx4. The rats were allowed to survive for a further 24 h (eight rats per group) (time 26 h). Behavioural tests were performed at this time point following the Longa neurological deficits scoring method. These rats were used for behavioural tests, immunohistochemistry, and infarcted areas measurement of ischemic injury.

TTC staining and quantification

TTC staining was performed 24 h after surgery. First, rat brain tissue was cut into five 2-mm thick sections starting from the frontal region. Then, tissue sections were stained using 2% TTC (DK0005, Leagene) solution at 37 °C for 30 min and fixed with 4% paraformaldehyde (J19943.K2 Thermo Fisher Scientific). Image Pro Plus 6 software (https://mediacy.com/image-pro/life-science-package/) was used to calculate the area percentages of normal tissue (dark red regions) and infarcted areas (white regions). For infraction area evaluation, three out of eight animals was randomly picked for staining. For TTC staining quantification, five sections of each animal were taken, and five sections per animal were used. Images were taken with a Canon PC1304 camera. TTC staining data was quantified with Image Pro Plus 6 software. (1) combines all raw images into one. (2) Segmentation: The color cube-based method uses transparency in black mode with a drop to create the preview image to extract the region of interest. (3) Counting size total: HSI mode with manual selection to select the total area of each brain slide, and then measure the area (start over 1000) and save data to file. (4) Count the size of infarction: threshold of saturation 0 ~45 and threshold of 150 ~255 was set. (5) Count the percentage of infarction with the formula: infarct percentage = 100 * infarction area/total area. Six microscopic images were taken for each animal (three for 100x and three for 400x).

H&E staining

At 24 h after administration of exosome and miRNA mimics, rats were deeply anaesthetized with 3% pentobarbital sodium (P3761 Sigma-Aldrich), and then normal saline and 4% paraformaldehyde were perfused into the heart. The brains were then removed and cut into sections (5 μm thick) and stained with H&E. Histological changes were analyzed using a LEICA microscope.

Neurological severity score and behavioral testing

The neurological deficits of mice were assessed following the method described (45) by Longa *et al.* 24 h after exosome and miRNA mimics administration by an investigator blinded to the experimental groups. The Longa score was assessed as follows: 0, no neurological deficit, normal walking; 1, mild neurological deficit, failure to fully extend contralateral forepaw; 2, moderate neurological deficit, circling to the contralateral side; 3, severe neurological deficit, falling to the contralateral side; 4, no spontaneous moving with depressed consciousness level. Rats with a score of 0 or 4 were excluded from this study. For neurological severity score and behavioral testing, 4 out of 8 animals per group were randomly picked and analyzed.

Data availability

The data and analysis code supporting the findings of this study are available from the corresponding author (Bingnan Li bingnan.li@sdu.edu.cn) upon reasonable request. Small RNA-seq data for exosomes of different MSCs from recent studies including at least three individuals was downloaded from the Gene Expression Omnibus database. For a single-cell dataset, we chose the datasets from the latest publication that included a similar MCAO animal model. Data cited in this paper are from GSE227651 (20), GSE195634, GSE153752 (31), and GSE159814 (16, 17). Small RNA-seq data for exosomes of different MSCs from recent studies including at least three individuals was downloaded from the Gene Expression Omnibus database. For the single-cell dataset, we chose the datasets from the latest publication that includes a similar MCAO animal model.

For reviewers, we generate the reviewer link for our RNA-seq datasets https://ngdc.cncb.ac.cn/gsa/s/L65WiPAY in Genome Sequence Archive and miRNA datasets https://ngdc.cncb.ac.cn/gsa-human/s/6bt3fDu6 in Genome Sequence Archive human.

References

1. Nargesi, A. A., Lerman, L. O., and Eirin, A. (2017) Mesenchymal stem cell-derived extracellular vesicles for kidney repair: current status and looming challenges. *Stem Cell Res. Ther.* **8**, 273
2. Chen, Q., Liu, Y., Ding, X., Li, Q., Qiu, F., Wang, M., *et al.* (2020) Bone marrow mesenchymal stem cell-secreted exosomes carrying microRNA-125b protect against myocardial ischemia reperfusion injury via targeting SIRT7. *Mol. Cell. Biochem.* **465**, 103–114
3. Cai, G., Cai, G., Zhou, H., Zhuang, Z., Liu, K., Pei, S., *et al.* (2021) Mesenchymal stem cell-derived exosome miR-542-3p suppresses inflammation and prevents cerebral infarction. *Stem Cell Res. Ther.* **12**, 2
4. Kuang, Y., Zheng, X., Zhang, L., Ai, X., Venkataramani, V., Kilic, E., *et al.* (2020) Adipose-derived mesenchymal stem cells reduce autophagy in stroke mice by extracellular vesicle transfer of miR-25. *J. Extracell. Vesicles* **10**, e12024
5. Zagrean, A.-M., Hermann, D. M., Opris, I., Zagrean, L., and Popa-Wagner, A. (2018) Multicellular Crosstalk between exosomes and the Neurovascular Unit after cerebral ischemia. Therapeutic Implications. *Front. Neurosci.* **12**, 811
6. Xin, H., Katakowski, M., Wang, F., Qian, J.-Y., Liu, X. S., Ali, M. M., *et al.* (2018) MicroRNA-17–92 cluster in exosomes enhance Neuroplasticity and functional recovery after stroke in rats. *Stroke* **48**, 747–753
7. Zhang, Z., Zou, X., Zhang, R., Xie, Y., Feng, Z., Li, F., *et al.* (2021) Human umbilical cord mesenchymal stem cell-derived exosomal miR-146a-5p reduces microglial-mediated neuroinflammation via suppression of the IRAK1/TRAF6 signaling pathway after ischemic stroke. *Aging(Albany NY)* **13**, 3060–3079
8. Xiong, Z.-G., Zhu, X.-M., Chu, X.-P., Minami, M., Hey, J., Wei, W.-L., *et al.* (2004) Neuroprotection in ischemia blocking calcium-Permeable acid-sensing ion channels. *Cell* **118**, 687–698
9. Wemmie, J. A., Taugher, R. J., and Kreple, C. J. (2013) Acid-sensing ion channels in pain and disease. *Nat. Rev. Neurosci.* **14**, 461–471
10. Yermolaieva, O., Leonard, A. S., Schnizler, M. K., Abboud, F. M., and Welsh, M. J. (2004) Extracellular acidosis increases neuronal cell calcium by activating acid-sensing ion channel 1a. *Proc. Natl. Acad. Sci. U. S. A.* **101**, 6752–6757
11. Wang, Y.-Z., Wang, J.-J., Huang, Y., Liu, F., Zeng, W.-Z., Li, Y., *et al.* (2015) Tissue acidosis induces neuronal necroptosis via ASIC1a channel independent of its ionic conduction. *Elife* **4**, e05682
12. Wang, J.-J., Liu, F., Yang, F., Wang, Y.-Z., Qi, X., Li, Y., *et al.* (2020) Disruption of auto-inhibition underlies conformational signaling of ASIC1a to induce neuronal necroptosis. *Nat. Commun.* **11**, 475
13. Redd, M. A., Scheuer, S. E., Saez, N. J., Yoshikawa, Y., Chiu, H. S., Gao, L., *et al.* (2021) Therapeutic inhibition of acid-sensing Ion Channel 1a

Recovers heart function after ischemia–reperfusion injury. *Circulation* **144**, 947–960

14. Kowal, J., Arras, G., Colombo, M., Jouve, M., Morath, J. P., Primdal-Bengtson, B., *et al.* (2016) Proteomic comparison defines novel markers to characterize heterogeneous populations of extracellular vesicle subtypes. *Proc. Natl. Acad. Sci. U. S. A.* **113**, E968–E977

15. Soni, N., Gupta, S., Rawat, S., Krishnakumar, V., Mohanty, S., and Banerjee, A. (2021) MicroRNA-enriched exosomes from different Sources of mesenchymal stem cells can differentially modulate functions of Immune cells and Neurogenesis. *Biomedicines* **10**, 69

16. Wang, Y., Lai, X., Wu, D., Liu, B., Wang, N., and Rong, L. (2021) Umbilical mesenchymal stem cell-derived exosomes facilitate spinal cord functional recovery through the miR-199a-3p/145-5p-mediated NGF/TrkA signaling pathway in rats. *Stem Cell Res. Ther.* **12**, 117

17. Tian, S., Zhou, X., Zhang, M., Cui, L., Li, B., Liu, Y., *et al.* (2022) Mesenchymal stem cell-derived exosomes protect against liver fibrosis via delivering miR-148a to target KLF6/STAT3 pathway in macrophages. *Stem Cell Res. Ther.* **13**, 330

18. Kim, C. G., Lee, J. K., Cho, G.-J., Shin, O. S., and Gim, J.-A. (2022) Small RNA sequencing of small extracellular vesicles secreted by umbilical cord mesenchymal stem cells following replicative senescence. *Genes Genom* **45**, 347–358

19. Pignataro, G., Simon, R. P., and Xiong, Z.-G. (2007) Prolonged activation of ASIC1a and the time window for neuroprotection in cerebral ischaemia. *Brain* **130**, 151–158

20. Zeng, F., Cao, J., Hong, Z., Liu, Y., Hao, J., Qin, Z., *et al.* (2023) Single-cell analyses reveal the dynamic functions of Itgb2+ microglia subclusters at different stages of cerebral ischemia-reperfusion injury in transient middle cerebral occlusion mice model. *Front. Immunol.* **14**, 1114663

21. Montecalvo, A., Larregina, A. T., Shufesky, W. J., Stolz, D. B., Sullivan, M. L. G., Karlsson, J. M., *et al.* (2012) Mechanism of transfer of functional microRNAs between mouse dendritic cells via exosomes. *Blood* **119**, 756–766

22. Santos, J. C., Lima, N. D. S., Sarian, L. O., Matheu, A., Ribeiro, M. L., and Derchain, S. F. M. (2018) Exosome-mediated breast cancer chemoresistance via miR-155 transfer. *Sci. Rep.* **8**, 829

23. Zheng, B., Yin, W., Suzuki, T., Zhang, X., Zhang, Y., Song, L., *et al.* (2017) Exosome-mediated miR-155 transfer from Smooth Muscle cells to endothelial cells induces endothelial injury and Promotes atherosclerosis. *Mol. Ther.* **25**, 1279–1294

24. Morelli, M. B., Shu, J., Sardu, C., Matarese, A., and Santulli, G. (2019) Cardiosomal microRNAs are essential in post-infarction myofibroblast Phenoconversion. *Int. J. Mol. Sci.* **21**, 201

25. Gambardella, J., Coppola, A., Izzo, R., Fiorentino, G., Trimarco, B., and Santulli, G. (2021) Role of endothelial miR-24 in COVID-19 cerebrovascular events. *Crit. Care* **25**, 306

26. Wang, X., Morelli, M. B., Matarese, A., Sardu, C., and Santulli, G. (2020) Cardiomyocyte-derived exosomal microRNA-92a mediates post-ischemic myofibroblast activation both in vitro and ex vivo. *ESC Heart Fail.* **7**, 285–289

27. Dewi, I. S., Celik, S., Karlsson, A., Hollander, Z., Lam, K., McManus, J.-W., *et al.* (2017) Exosomal miR-142-3p is increased during cardiac allograft rejection and augments vascular permeability through down-regulation of endothelial RAB11FIP2 expression. *Cardiovasc. Res.* **113**, 440–452

28. Chuang, H.-Y., Su, Y., Liu, H.-W., Chen, C.-H., Chiu, S.-C., Cho, D.-Y., *et al.* (2019) Preclinical evidence of STAT3 inhibitor Pacritinib Overcoming Temozolomide resistance via downregulating miR-21-enriched exosomes from M2 Glioblastoma-associated macrophages. *J. Clin. Med.* **8**, 959

29. Huang, P., Wang, L., Li, Q., Xu, J., Xu, J., Xiong, Y., *et al.* (2019) Combinatorial treatment of acute myocardial infarction using stem cells and their derived exosomes resulted in improved heart performance. *Stem Cell Res. Ther.* **10**, 300

30. Birtwistle, L., Chen, X.-M., and Pollock, C. (2021) Mesenchymal stem cell-derived extracellular vesicles to the rescue of renal injury. *Int. J. Mol. Sci.* **22**, 6596

31. Dong, C., Chen, M., Cai, B., Zhang, C., Xiao, G., and Luo, W. (2022) Mesenchymal stem cell-derived exosomes improved cerebral infarction via transferring miR-23a-3p to activate microglia. *Neuromolecular Med.* **24**, 290–298

32. Moon, S., Shin, D. W., Kim, S., Lee, Y.-S., Mankhong, S., Yang, S. W., *et al.* (2019) Enrichment of exosome-like extracellular vesicles from plasma suitable for clinical Vesicular miRNA biomarker research. *J. Clin. Med.* **8**, 1995

33. Zhang, J., Yang, J., Wang, H., Sherbini, O., Keuss, M. J., Umanah, G. K., *et al.* (2018) The AAA + ATPase Thorase is neuroprotective against ischemic injury. *J. Cereb. Blood Flow Metab.* **39**, 1836–1848

34. Kim, D., Langmead, B., and Salzberg, S. L. (2015) HISAT: a fast spliced aligner with low memory requirements. *Nat. Methods* **12**, 357–360

35. Pertea, M., Kim, D., Pertea, G. M., Leek, J. T., and Salzberg, S. L. (2016) Transcript-level expression analysis of RNA-seq experiments with HISAT, StringTie and Ballgown. *Nat. Protoc.* **11**, 1650–1667

36. Robinson, M. D., and Oshlack, A. (2010) A scaling normalization method for differential expression analysis of RNA-seq data. *Genome Biol.* **11**, R25

37. Robinson, M. D., McCarthy, D. J., and Smyth, G. K. (2010) edgeR: a Bioconductor package for differential expression analysis of digital gene expression data. *Bioinformatics* **26**, 139–140

38. Langmead, B., Trapnell, C., Pop, M., and Salzberg, S. L. (2009) Ultrafast and memory-efficient alignment of short DNA sequences to the human genome. *Genome Biol.* **10**, R25

39. Kozomara, A., and Griffiths-Jones, S. (2014) miRBase: annotating high confidence microRNAs using deep sequencing data. *Nucleic Acids Res.* **42**, D68–D73

40. Ru, Y., Kechris, K. J., Tabakoff, B., Hoffman, P., Radcliffe, R. A., Bowler, R., *et al.* (2014) The multiMiR R package and database: integration of microRNA–target interactions along with their disease and drug associations. *Nucleic Acids Res.* **42**, e133

41. Gu, Z., Gu, L., Eils, R., Schlesner, M., and Brors, B. (2014) Circlize implements and enhances circular visualization in R. *Bioinformatics* **30**, 2811–2812

42. Wu, T., Hu, E., Xu, S., Chen, M., Guo, P., Dai, Z., *et al.* (2021) clusterProfiler 4.0: a universal enrichment tool for interpreting omics data. *Innovation* **2**, 100141

43. Walter, W., Sánchez-Cabo, F., and Ricote, M. (2015) GOplot: an R package for visually combining expression data with functional analysis. *Bioinformatics* **31**, 2912–2914

44. Dirnagl, U., and Members of the MCAO-SOP Group (2010) Standard operating procedures (SOP) in experimental stroke research: SOP for middle cerebral artery occlusion in the mouse. *Nat. Précéd.* https://doi.org/10.1038/npre.2010.3492.2

45. Longa, E. Z., Weinstein, P. R., Carlson, S., and Cummins, R. (2018) Reversible middle cerebral artery occlusion without craniectomy in rats. *Stroke* **20**, 84–91